MULTI-TEMPORAL ANALYSIS OF AMBIENT NOISE POLARIZATION TO CHARACTERIZE SITE RESPONSE IN THE TOWN OF AMATRICE, SHATTERED BY THE 2016 CENTRAL ITALY EARTHQUAKE

Vincenzo Del Gaudio[a*], Janusz Wasowski[b], Pierpaolo Pierri[a], Antonio Moretti[c], Gianluca Ferrini[c],

[a] Dipartimento di Scienze della Terra e Geoambientali, Università degli Studi di Bari "Aldo Moro"– Bari, Italy

[b] Consiglio Nazionale delle Ricerche – Istituto di Ricerca per la Protezione Idrogeologica - Bari, Italy

[c] Dipartimento di Medicina Clinica, Sanità Pubblica, Scienze della Vita e dell'Ambiente, Università degli Studi dell'Aquila, Italy

* Corresponding author – email: vincenzo.delgaudio@uniba.it

Abstract

The Mw 6.0 earthquake that hit central Italy on 24 August 2016 caused an abnormally high level of destruction in the town of Amatrice. In order to clarify the role of site response in causing such a disaster, a series of ambient noise recordings acquired in the aftermath of the event are analysed here to identify site resonance properties from the ratios H/V between horizontal and vertical amplitudes of ground motion. Although the noise data acquisition was limited by the emergency management activities, the use of a new analysis technique, which isolates the contribution of Rayleigh waves to the noise wavefield and averages instantaneous estimates of H/V ratios, provided more stable results compared to the standard Nakamura's technique based on mean spectral ratios. The results demonstrated the occurrence of significant resonance phenomena, but without an obvious correlation with the spatial distribution of damage severity. It is apparent that the damage severity was also influenced by some additional local factors related to building vulnerability. Moreover, the time series analysis revealed seasonal variations in the Rayleigh wave ellipticity curves likely related to the water content changes in the surface deposits and their influence on the Poisson coefficient. Finally, the new method proved capable of recognizing time-varying directions of Rayleigh wave propagation. This capability could be exploited to support other passive seismic methods (e.g. ReMi), whose results reliability is limited by the lack of control on wave direction origin.

Keywords: Earthquake ground motions, Earthquake hazards, Site effects, Seismic noise, Time series analysis, Surface waves and free oscillations.

1. Introduction

Starting from 24 August 2016, central Italy was shaken by a seismic sequence that, after the first shock of moment magnitude Mw 6.0 (epicentre 1 km away from the village of Accumoli, Lazio region), reached a maximum on 30 October 2016 with a shock of Mw 6.5 (epicentre 4 km away from the town of Norcia, Umbria region) (Fig. 1). The first Mw 6.0 shock severely damaged the town of Amatrice distant about 10 km from the epicentre. The extent of damage was abnormally high for an Italian earthquake of such a magnitude. Collapses of buildings in the Amatrice's old town centre accounted for more than 3/4 of the 300 victims caused by this

earthquake. Different factors could have contributed to such a large number of fatalities, including building vulnerability and local amplification of ground motion. Therefore, in view of the post-earthquake reconstruction of the town, it is of the utmost importance to clarify the reasons of this disaster.

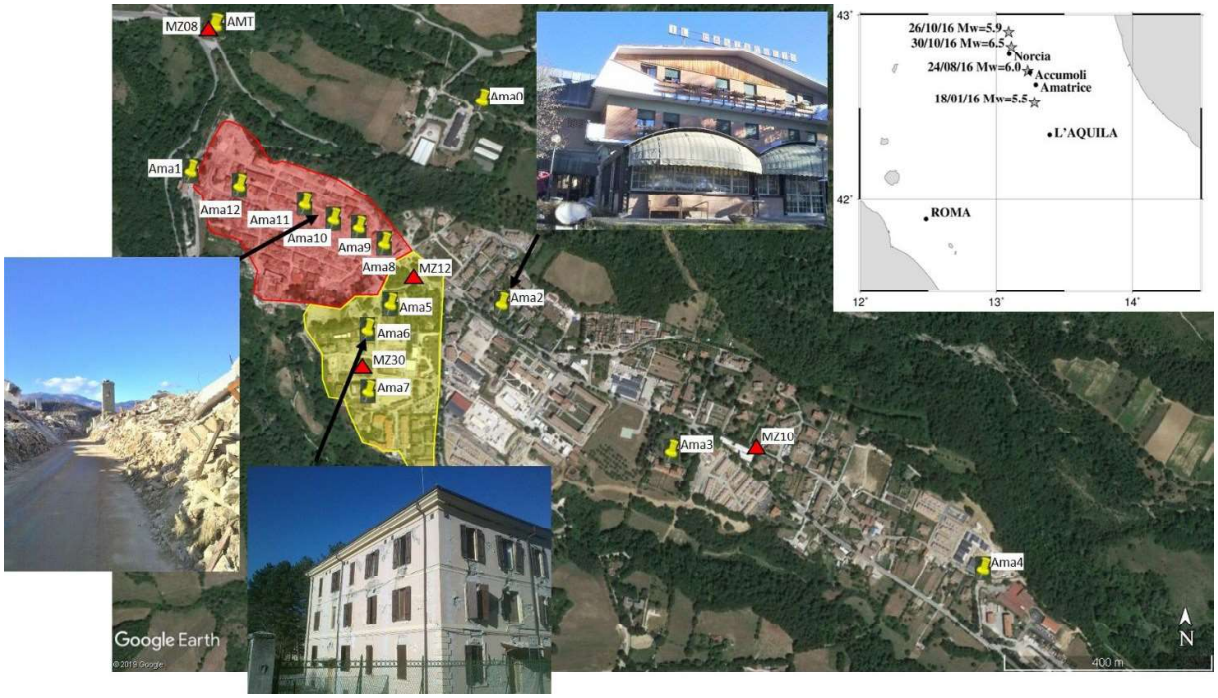

Fig. 1 – Google Earth image of the town of Amatrice with the location of the sites of ambient noise measurements Ama0-12 and the accelerometer station AMT of the Italian National Accelerometer Network (yellow pushpins). Note also four temporary accelerometer stations MZ08-10-12-30 (red triangles) whose earthquake recordings were used in the study of Milana et al. (2019). Photos from left to right illustrate earthquake effects in the "Red zone", "Yellow zone" and in the less damaged area, respectively. The top right inset shows the geographical locations of Amatrice and other towns hit by the 2016-2017 seismic sequence. Grey stars mark the epicentres of the major shocks (Mw ≥ 5.5), with the indication of date and magnitude (data from Istituto Nazionale di Geofisica e Vulcanologia - http://terremoti.ingv.it/).

The damage severity was anything but homogeneous in the urbanized area of Amatrice. Complete destructions occurred in the north-western part of the town, classified as "Red zone", corresponding to the Amatrice historic centre, whereas severe damage, generally without building collapses, was observed in the south-central part of the town, classified as "Yellow zone" (Fig. 1). The remaining and more recent built-up areas (central and eastern urban parts of the town), suffered relatively lighter damage during the first major shock. However, the cumulative effects of this and the following shocks led to severe damage also in these parts of the town.

The re-building of Amatrice poses one crucial question concerning the role of site response in aggravating the earthquake effects in different parts of the town. At this regard, Milana et al. (2019) presented the results of extensive investigations started in the aftermath of the seismic sequence and conducted until the end of 2017. However, data acquisition during a seismic crisis could be hampered during the emergency management actions, which can limit the access to the study area and the applicability of some investigation techniques. In this context, the analysis of ambient noise, i.e., persistent ground vibration due to non-seismic sources (winds, sea waves, machinery, road traffic), can provide timely information for site response characterization.

Ambient noise can be recorded through stand-alone station measurements using lightweight, compact seismographs: this allows a quick acquisition of data even within the context of an area that is coping with the problems of emergency management. However, complex geological settings, together with the presence of noise wavefield strongly disturbed by civil protection activities, pose limitations to the use of standard techniques of noise analysis such as the method of horizontal-to vertical spectral ratios (Nakamura 1989). The limitations can result from the presence of uncontrolled sources of noise variability and uncertainties about the actual composition of the noise wavefield, which reduce the amount and the reliability of information these standard techniques can provide (cf. Bonnefoy-Claudet et al. 2006; Del Gaudio et al. 2014).

Hence, in Amatrice we tested the potential of a new technique based on instantaneous analysis of signal polarization (Del Gaudio 2017), originally developed for investigating complex site conditions e.g., considerable topographic relief and lateral heterogeneities or anisotropy of subsoil properties. Our test relied on a series of ambient noise acquisitions from October 2016 to June 2018. We used four tromographs, i.e., compact lightweight meters specifically devised for noise recordings. We acquired noise data at different times and in different periods of the year in order to evaluate the stability of the results and to verify the possible presence of variations related to seasonal factors.

Furthermore, the measurements covered a period during which site conditions have undergone modifications due to the works aimed at restoring the urban area, including the demolition of irreparably damaged buildings and the removal of rubble. At some sites the measurements were carried out both before and after the demolition of nearby buildings, and this provided the opportunity of verifying the influence of building vibrations on the ambient noise recorded in urban areas for site response investigations (cf., Gallipoli et al. 2004).

2. Geological setting

Amatrice lies within a wide inter-mountain basin of Upper Pleistocene age, delimited to the north-east by a major normal fault bordering the flank of Mount Gorzano (Fig. 2). The fault provided the best evidence of reactivation during the earthquake of 30 October 2016. The sedimentary fill of the basin has a limited thickness (60 m at most) and consists of Quaternary alluvial deposits, locally forming terraces.

The north-eastern part of the basin, which includes Amatrice, is formed by a series of large morphological terraces, covered by few tens of meters of torrential or fluvio-lacustrine deposits. These predominantly pebbly deposits extend towards the valley of the river Tronto, which cuts through the thin sedimentary cover to the underlying arenaceous-marly rocks of the Tertiary age Laga Flysch.

The Amatrice plain, in particular, is covered by 30-35 meters of sediments, mainly conglomerates with intercalations of grey or brown clays at the base, which progressively turn to pebbly-gravely levels, with smaller and more rounded pebbles, sands and clear pelitic horizons. The uppermost part of the succession is generally represented by 5-10 m of reddish or yellowish micaceous siltstone of probable aeolian origin.

3. Data acquisition

Noise recordings were acquired using three tromographs model “Tromino” (see www.moho.world/Tromino for technical details) in the first campaigns and four in the last one. During measurements, one of the tromographs was kept continuously recording at a “reference” station, while the others were used for 30-46 minute-long measurement sessions. In this way, it is possible to distinguish whether differences in ambient noise properties acquired by different stations at different times reflect spatial changes in site-specific characteristics of soil dynamic response or depend on temporal changes of environmental conditions controlling the noise wavefield.

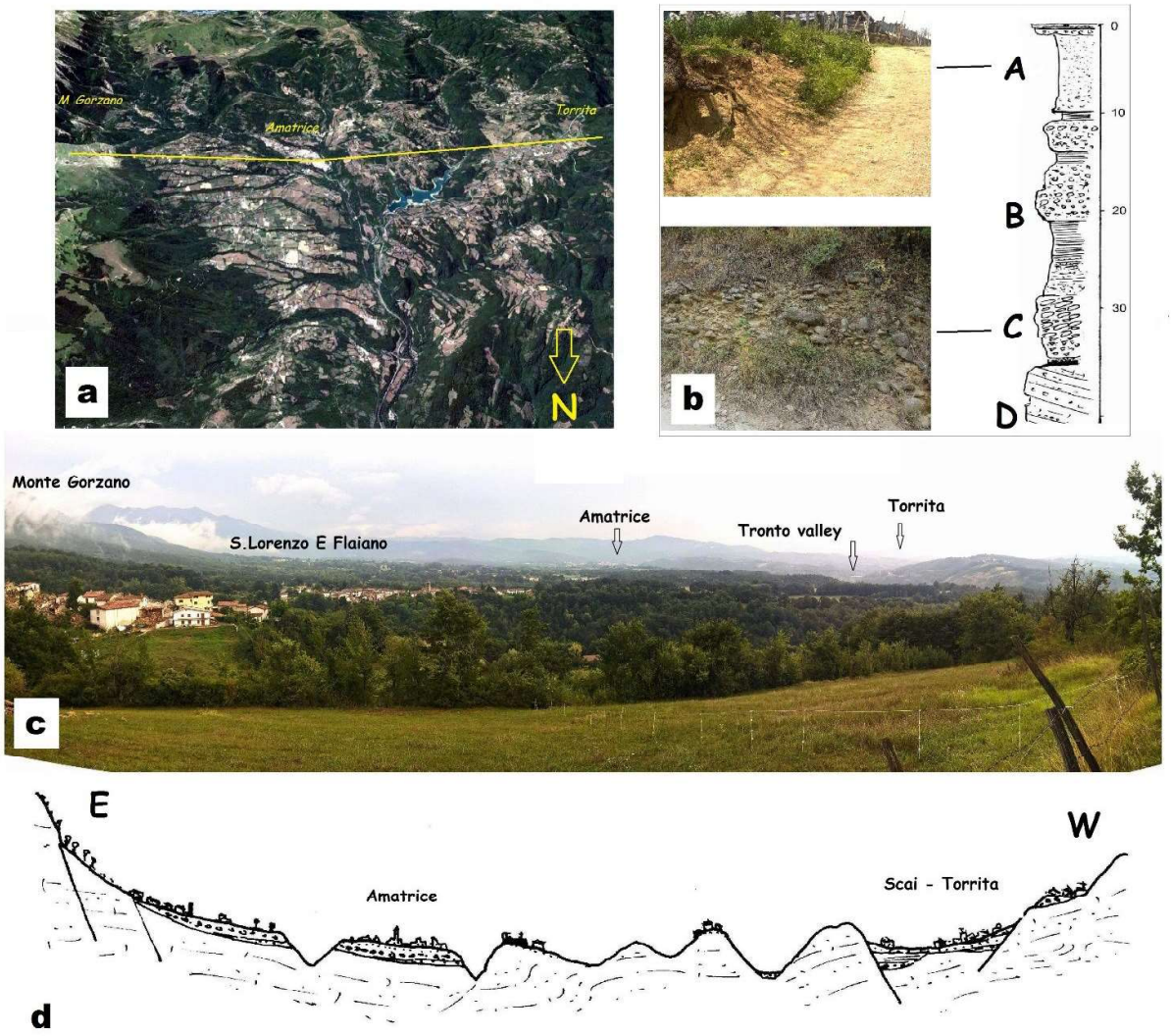

Fig. 2 – Geology of the Amatrice inter-mountain basin in central Italy. a) Google Earth image of the basin illustrating the distribution of Pleistocene-Holocene age deposits. Lighter colour alluvial fan deposits originating at the base of the Mount Gorzano are easily distinguished in the eastern (left) part of the figure. These up to 20-40 m thick deposits are dissected by many torrents that locally reach the substratum (Tertiary age Laga Flysch). b) Stratigraphic column reconstructed on the basis of two boreholes drilled in the vicinity of Ama6 station (cf., Fig. 1): A – Fine grained, silty yellowish sands of likely late-glacial aeolian origin (5-10 m). B – Greyish silty clays with light coloured sandy intercalations, poorly cemented, passing to few meter thick beds of moderately sorted conglomerates, often mud-supported (10-20 m). C) Coarse conglomerates, clast-supported, with sub-rounded and often imbricated clasts (5-10 m). The transition to the underlying arenaceous-marly substratum is sharp and often of erosional nature. D) Conglomerate, sandstone and marl alternations (Tertiary age flysch substratum), strongly weathered in the upper part. c) Overview of the Amatrice basin (view towards the south). d) Schematic, not to scale geological section; Fig. 2a shows the section location.

Noise recordings were acquired on four different dates. The first measurements were carried out in October 2016 at a site located close to the western boundary of the "Red zone" (Ama1) and at three sites located outside the most damaged zones (Ama2, Ama3, Ama4); the scope was to obtain an approximately NW-SE profile across the urban area. Initially, a site located outside the urban area (Ama0) was used as a reference. However, the first analyses suggested the presence of apparently lower amplification effects at site Ama2 than at Ama0, and in subsequent recordings, Ama2 was used as reference. In December 2016, having been authorized to conduct investigations in the most damaged zones, noise recordings were acquired at four additional sites (Ama8, Ama9, Ama10, Ama11) in the Red zone, following approximately the same NW-SE alignment of the previous measurements, and at three sites of the Yellow zone (Ama5, Ama6, Ama7) arranged to form a transversal profile (Fig. 1).

In April 2017, recordings were acquired at the same sites of the December 2016 measurement campaign, at the site Ama1 and at a new site (Ama12) in the Red zone, where measurements had not been previously possible for the presence of machinery at work. Finally, the last measurement campaign was conducted in June 2018, acquiring data at almost all the sites of the previous campaign (except for Ama5, due to access problems). In addition, the reference tromograph was deployed at the site of a station belonging to the Italian National Accelerometer Network and run by the Italian National Institute of Geophysics and Volcanology (see http://itaca.mi.ingv.it/). This station (AMT in Fig. 1) is located on an outcrop of massive sandstones of the Laga Flysch. For comparison purposes, the 2018 measurements included a long noise recording at Ama2 as well, which had been used as reference in the previous campaigns.

4. Analysis methodology

Ambient noise data acquired in this area were processed following both the traditional Nakamura's approach (Nakamura 1989) and a recently proposed HVIP - Horizontal-to-Vertical ratios from Instantaneous Polarization analysis (Del Gaudio 2017). The Nakamura's approach calculates the average spectral ratios HVNR between horizontal and vertical component of noise recording. It was implemented following the recommendations of the project SESAME (Site EffectS assessment using Ambient Excitations: see Bard & the SESAME Team, 2004). Consequently, recordings were subdivided into time windows of 20 s, excluding

from the analysis the time intervals during which spectral ratios were significantly different from the average. Spectra obtained from each time window were first smoothed using the function proposed by Konno & Ohmachi (1998), and then spectral ratio H/V between horizontal and vertical components were calculated and averaged over the different time windows. To examine directional variations of spectral ratios, the HVNR values were calculated along different horizontal directions at azimuth intervals of 10°. It is generally reckoned that this method cannot provide a direct measure of the amplification factor but only an estimate of the fundamental resonance frequency (Bard 1999; Perron et al. 2018). Moreover, if a site response directivity is present, the direction of maximum amplification can be obtained (Del Gaudio et al. 2008).

The new HVIP technique uses instantaneous polarization analysis to identify packets of Rayleigh waves within the noise recording and determines their ellipticity (intended as the ratio between the horizontal H and vertical V component of elliptical particle motion), together with the azimuth of the vertical plane containing the elliptical motion. According to this method, a noise recording is passed through narrow-band filters centred on different frequencies and an analytic transformation is applied to the filtered time series to infer instant-by instant polarization properties. In particular, ground motion can be described at each instant as part of an elliptical trajectory whose axes can be derived from the formulae published by Morozov and Smithson (1996). Rayleigh wave packets are recognized when a sequence of recording samples shows coherent elliptical trajectories lying on subvertical planes, whose principal axes are horizontally and vertically directed. The method can provide thousands of instant-by-instant estimates of H/V ratios from polarization properties of ground motion, isolating the portions of noise recordings where Rayleigh waves are dominant and then inferring curves of Rayleigh wave ellipticity as function of frequency, smoothed through the Konno & Ohmachi (1998) filter. Such curves can be related to site response properties like site resonance frequency, which typically shows a maximum of Rayleigh wave ellipticity oriented according to the site response directivity. Furthermore, the peak amplitudes of the ellipticity curves, if subjected to smoothing, are correlated to the amplification factors, in that both depend on the velocity contrast between bedrock and surface layer (Konno and Ohmachi 1998). The ellipticity curves can give indirect information on subsoil properties responsible of local variations of site amplification, and thus help constrain, with the support of additional data, subsoil velocity models (c.f. Castellaro & Mulargia 2009). These could in turn be used to calculate the amplification factor from numerical simulation of the site response.

5. Results

The results of the analyses of ambient noise recordings are summarized in Tables 1 - 2 and discussed focusing on the different parts of the urban area. The tables report frequency, amplitude and direction of major peaks identified from the HVNR curves (Table 1) or the HVIP curves (Table 2) in the different measurement campaigns, together with the ratio R between the directional maximum and minimum of the H/V values (spectral ratios or Rayleigh wave ellipticity) at the peak frequencies. This ratio was used as index to characterize the site response directivity: R values lower than 1.5 were considered as indicative of the absence of significant directional variations in the site response properties (cf. Del Gaudio et al. 2008). The peaks listed in Tables 1-2 are the largest ones that showed similar characteristics in different campaigns. Peaks recognized only in one campaign were not considered indicative of site response properties, but dependent on temporary properties of the noise wavefield and, therefore, neglected.

Table 1: *Peak values of H/V spectral ratios derived from the HVNR analysis of ambient noise recording in the four measurement campaigns: f = frequency (in Hz) of peak value; A = H/V peak value; Az = azimuth of directional maximum (degrees from North); R = ratio between directional maximum and minimum at the frequency f.*

Sta	2016 October				2016 December				2017 April				2018 June			
	f(Hz)	A	Az	R	f(Hz)	A	Az	R	f(Hz)	A	Az	R	f(Hz)	A	Az	R
AMT													4.75	3.2	115°	3.0
Ama0	5.80	4.5	135°	1.3												
Ama1	3.45	3.8	175°	1.3					3.20	9.8	155°	1.7	3.30	6.7	135°	1.1
Ama2	2.75	2.5	155°	1.5	2.45	3.4	135°	1.9	2.55	3.5	135°	2.3	2.50	2.6	115°	1.3
	4.00	2.6	165°	1.8	3.10	3.5	135°	1.9	3.25	3.6	125°	2.0	3.45	2.7	115°	1.5
	10.40	3.0	165°	1.2	9.40	2.9	25°	1.1	9.55	2.9	35°	1.2	8.95	2.9	5°	1.2
Ama3	3.70	2.6	135°	2.0									2.45	2.3	165°	1.7
Ama4	2.50	3.4	125°	1.6									2.35	3.0	145°	1.8
Ama5					2.35	3.9	115°	2.1	2.20	4.8	165°	2.8				
					9.15	3.4	105°	1.2	9.20	2.5	75°	1.1				
Ama6					2.25	5.0	145°	2.4	3.00	6.3	145°	4.1	3.15	3.0	135°	1.6
Ama7					2.35	4.4	105°	1.6	2.85	5.6	135°	2.1	2.00	5.1	65°	1.7
					8.30	2.5	155°	1.7	8.35	2.0	155°	1.2	9.40	1.8	65°	1.4
Ama8					2.25	5.1	135°	2.5	2.60	4.2	175°	3.2	2.15	2.7	175°	1.3
Ama9					2.25	4.5	135°	2.4	2.45	2.2	145°	1.7	2.85	2.2	135°	1.3
					5.25	2.2	135°	1.5	4.70	1.6	125°	1.7	5.50	2.1	135°	1.2
Ama10					2.05	3.3	125°	2.1	3.25	3.3	135°	2.9	2.05	3.6	135°	1.5
Ama11					2.05	3.6	155°	2.0	2.25	1.7	135°	1.3	1.95	3.7	45°	2.5
					5.15	2.8	165°	2.0	5.10	1.3	175°	1.1	5.90	1.7	45°	2.5
Ama12									3.95	3.8	125°	1.8	3.65	4.0	155°	1.4

Table 2: *Peak values of Rayleigh wave ellipticity curves derived from the HVIP analysis of ambient noise recordings in the four measurement campaigns: f = frequency (in Hz) of peak value; A = H/V peak value; Az = azimuth of directional maximum (degrees from North); R = ratio between directional maximum and minimum at the frequency f.*

Sta	2016 October				2016 December				2017 April				2018 June			
	f(Hz)	A	Az	R	f(Hz)	A	Az	R	f(Hz)	A	Az	R	f(Hz)	A	Az	R
AMT													4.85	4.0	125°	3.7
Ama0	5.90	4.5	165°	1.1												
Ama1	3.25	6.5	165°	6.1					3.40	6.5	155°	2.1	2.90	6.1	125°	2.0
Ama2	2.95	3.5	155°	1.5	2.50	4.3	135°	1.6	2.55	4.5	135°	1.9	2.40	3.7	135°	1.4
	4.95	3.9	155°	1.5	4.60	3.7	125°	1.4	4.85	3.4	125°	1.4	5.15	3.7	125°	1.4
	10.35	4.1	175°	1.2	10.1	3.4	165°	1.1	9.80	3.5	145°	1.0	10.4	3.6	135°	1.1
Ama3	2.05	3.2	85°	1.8									2.35	3.5	5°	3.1
Ama4	2.85	3.7	135°	2.0									2.70	3.5	145°	2.4
Ama5					2.35	4.4	125°	2.0	2.25	4.3	165°	2.1				
					9.20	4.2	105°	1.2	9.35	3.5	135°	1.1				
Ama6					2.75	4.6	155°	1.7	2.80	4.6	135°	2.2	3.05	4.3	165°	2.0
Ama7					1.90	4.4	145°	1.9	2.40	4.3	145°	1.7	2.20	4.6	135°	1.4
					8.65	3.6	165°	1.7	8.25	3.4	145°	1.4	8.50	3.0	135°	1.2
Ama8					2.00	5.3	135°	1.7	2.45	4.9	165°	2.3	2.10	4.2	135°	1.7
Ama9					2.35	4.2	145°	2.4	2.65	3.4	145°	2.6	2.00	3.8	145°	2.4
					5.25	3.6	115°	1.6	5.45	2.7	145°	1.7	5.90	3.9	155°	1.8
Ama10					3.20	4.1	105°	2.8	3.40	4.6	145°	8.7	3.05	4.1	105°	1.9
Ama11					2.55	3.9	165°	1.7	2.35	1.9	115°	4.4	2.35	4.4	125°	1.6
					5.05	3.5	165°	3.0	5.30	1.2	145°	2.0	4.70	3.4	145°	2.0
Ama12									3.70	3.8	135°	4.6	3.95	5.2	165°	1.6

5.1 Reference sites

Recordings at reference sites, prolonged for some hours, gave indications about the variability of noise wavefield during a single campaign and between different measurement campaigns. For the first campaign we initially used as reference the station Ama0 located on an alluvial terrace north of the Amatrice urban area (Fig. 1). However, data analysis, conducted using both the HVNR and HVIP methods, showed evidence of an important site amplification with an almost isotropic character at Ama0 (Fig. 3). This is reflected by high values of Rayleigh wave ellipticity, which are larger than 4 in a frequency band between 5 and 8 Hertz, with a peak of 4.5 at 5.9 Hz and R = 1.1 (Table 2).

Nevertheless, during the first campaign, a long recording was also acquired at site Ama2, located in the garden of an abandoned hotel (see the uppermost photo in Fig. 1). The results of the data analysis suggested that the site is affected by a lower amplification than Ama0 (lower peak values of H/V ratios: see Tables 1 and 2). This, together with the site proximity to the other measurement sites, made convenient its adoption as reference for the following campaigns. Figure 4 summarizes the results obtained at Ama2 in the four measurement campaigns.

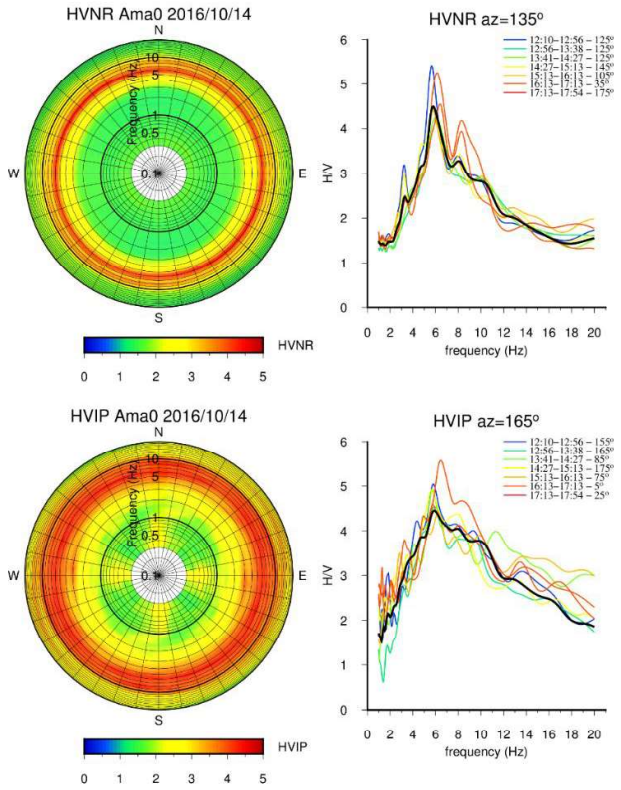

Fig. 3 – Polar diagrams (to the left) of mean spectral ratios calculated with the Nakamura approach (HVNR, at the top) and of Rayleigh wave ellipticity estimated with the HVIP technique (bottom) for the site Ama0. Diagrams to the right report the curve of HVNR (top) and HVIP (bottom) values along the azimuth of maximum H/V ratios (135° and 165°, respectively). Thick black lines represent the average over the entire duration of noise recording, whereas thinner colour lines show the curves of maximum H/V ratios obtained for different time intervals along different directions, as indicated in the legend.

Noise recordings were acquired in four different periods of the year (mid-October, mid-December, mid-April and end of June) and the results provided evidence of a complex pattern of site amplification, with resonances in two frequency bands, one, generally more pronounced and with a NW-SE directional character, between 2 and 5 Hz, and another more isotropic (R = 1.0 - 1.2) between 9 and 11 Hz. The amplitudes of peaks of Rayleigh wave ellipticity differ from those of spectral ratios (cf. Tables 1 and 2). Similar differences between the outcomes of the two methods were also observed in previous studies (e.g., Del Gaudio et al. 2018) as effect of the presence, within the noise wavefield, of other wave types combined in time-varying proportions with Rayleigh waves. The 2-5 Hz band seems also to have complex characteristics, with the possible lateral overlapping of two or more peaks. These peaks show a time variability that appears to follow a seasonal cycle, with larger amplitudes at relatively lower frequencies (closer to 2 Hz) in the two most rainy periods (at the end of autumn and in spring), and smaller peaks at higher frequencies (closer to 5 Hz) in the driest periods (summer-early autumn: see Fig. 4).

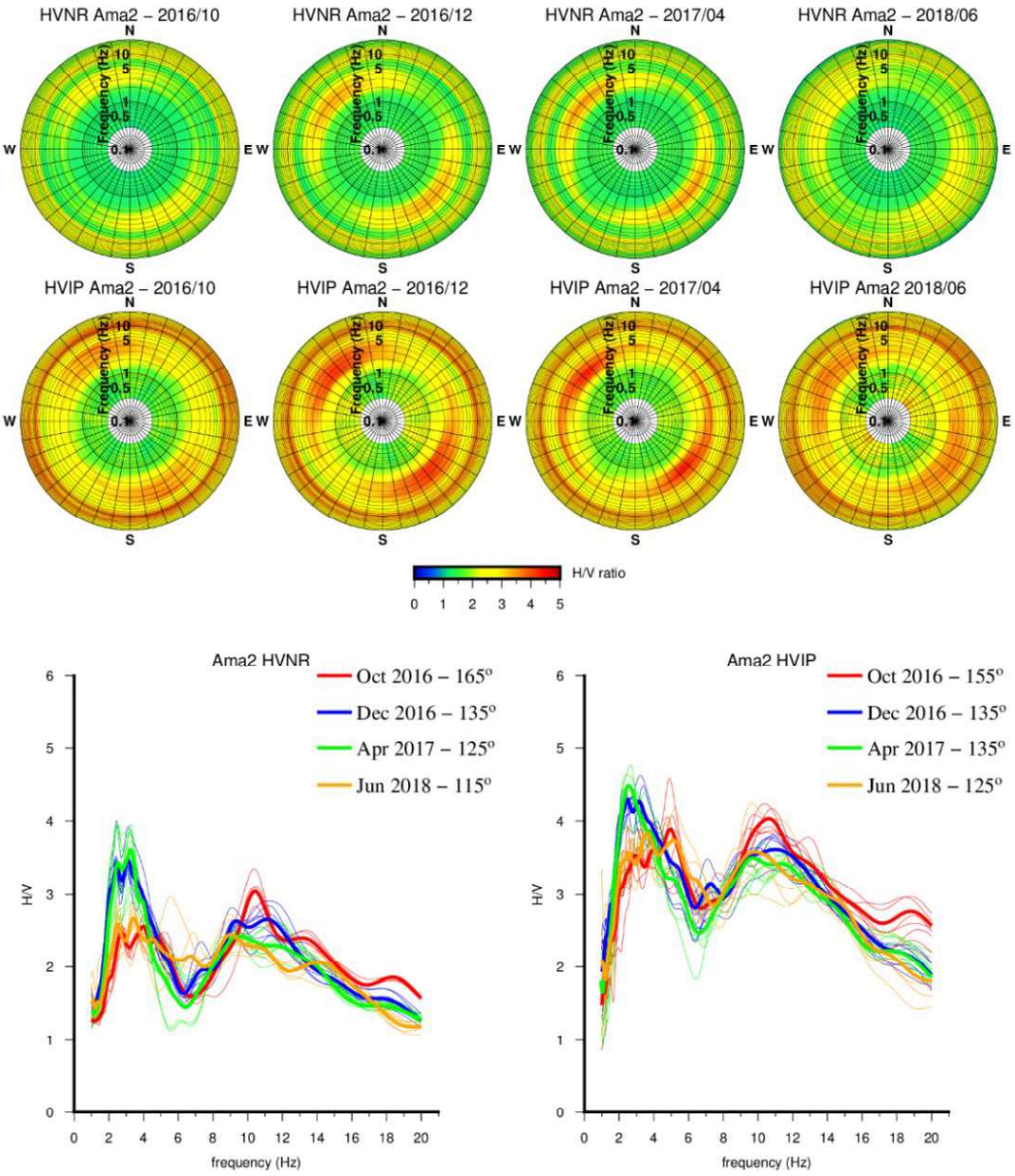

Fig. 4 – Polar diagrams of HVNR and HVIP values (top) obtained from the four measurement campaigns at site Ama2 and diagrams with their values along the azimuth of the maxima in the frequency band 2-5 Hz (bottom). Thick lines represent the average over the entire duration of noise recording, whereas thin lines show the results obtained for measurements at different time intervals.

In the last measurement campaign (end of June 2018), we tested the utility of another reference site, deploying one of the tromographs next to the accelerometer station AMT (Fig. 1), located on an outcrop of a massive sandstone (local substratum). The results of the noise data analysis are shown in Fig. 5.

The ellipticity data revealed the presence of resonance with properties similar to one of the peaks of the 2-5 Hz band of resonance at Ama2. The major peak found at AMT was due N125°E, at a frequency of 4.85 Hz with an amplitude of 4.0 (Fig. 5 and Table 2). Comparatively, at Ama2, the major Rayleigh wave ellipticity

peak between 2 and 5 Hz was found in October 2016 at 4.95 Hz with amplitude 3.9 and direction N155°E, whereas the second major peak in June 2018 was found at 5.15 Hz with an amplitude of 3.7 and a directional maximum in the same direction as at AMT (N125°E).

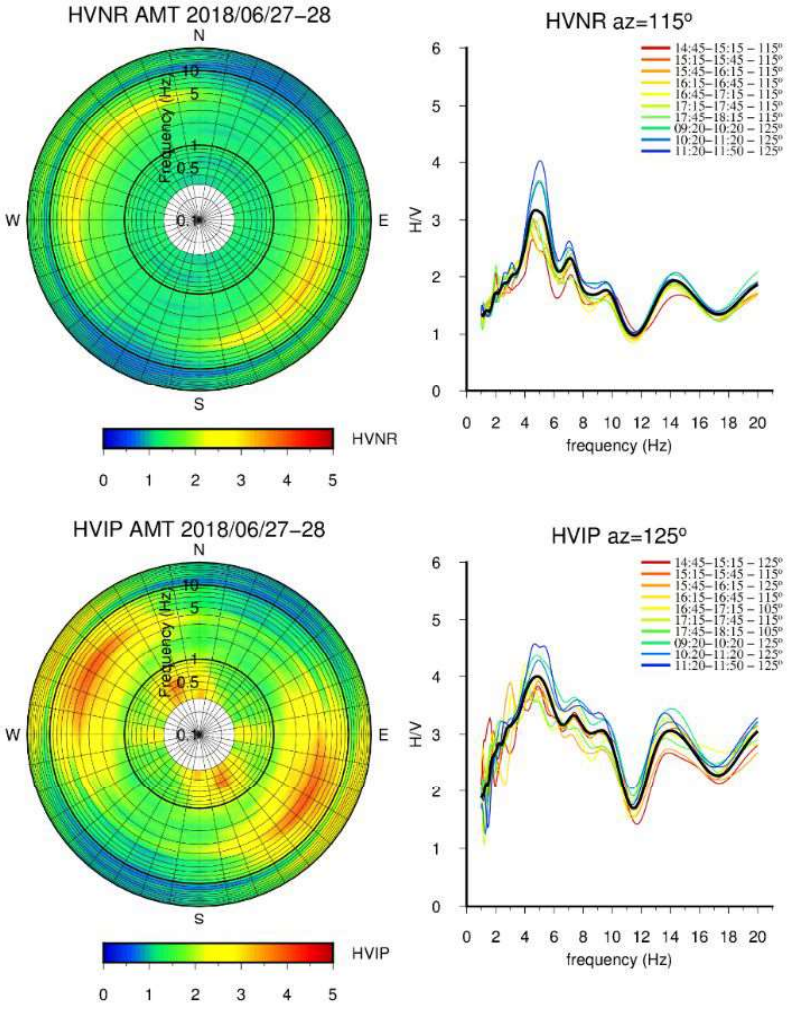

Fig. 5 – Polar diagrams of HVNR (top) and HVIP (bottom) values for the AMT site. Diagrams to the right report the curves H/V along the azimuths of major peaks (115° and 125°, respectively). Thick black lines represent the average over the entire duration of noise recording, whereas thinner colour lines show the curves of maximum H/V ratios obtained for different time intervals along different directions, as indicated in the legend.

In general, the peak amplitude variability at different time intervals of the same measurement campaign appeared more limited than seasonal variation, even though the outcomes of single recordings could differ considerably from the average (e.g. see in Fig. 3 the curve for the interval 17:13 - 17:54, relative to Ama0). The peak amplitudes estimated at Ama2 at different times of the day suggest variations possibly related to the reduction of traffic and anthropic activity at the central hours of the day (earlier in December, later in April and October (Fig. 6).

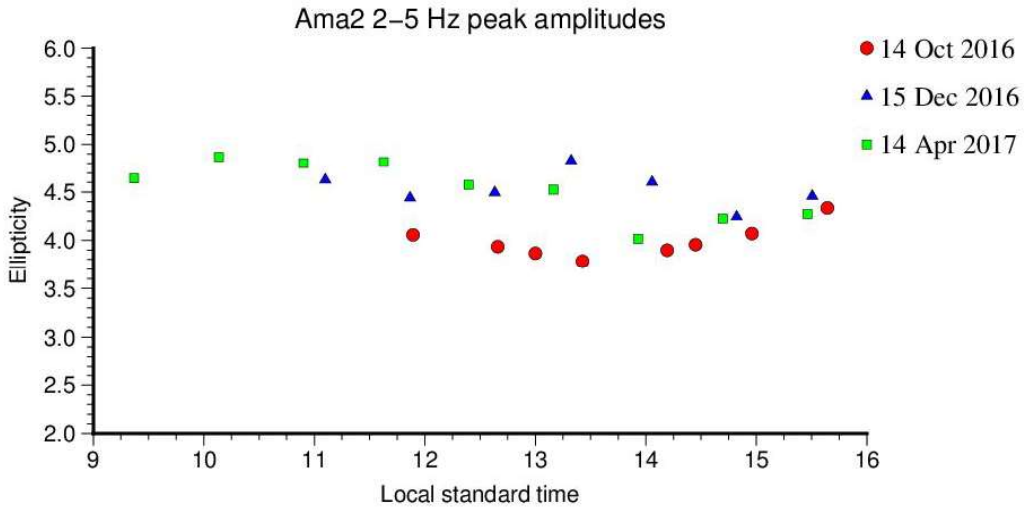

Fig. 6 – Temporal variations of amplitudes of maximum ellipticity for peak frequency between 2 and 5 Hz, resulting at the reference site Ama2 from the HVIP analysis at different times of the day (local standard time), during different measurement days.

5.2 The "Red" zone

The measurement sites in the Red zone of Amatrice were arranged along a virtual profile crossing the town's historical centre from NW to SE. The first site of the profile, named Ama1, was set up on conglomerates at the north-western periphery of the town, just outside the zone where free access was inhibited to population for safety reasons. Noise recordings were acquired here in October 2016, April 2017 and June 2018.

The data analysis showed the presence of a resonance at a peak frequency around 3 Hz. Although some other peaks appeared at lower frequencies, this was the only temporally persistent major peak. Therefore, the peak can be interpreted as a site-specific characteristic of H/V ratios, not depending on temporal variations of noise sources. Peak frequency was consistent during the three measurement campaigns, resulting respectively 3.45, 3.20 and 3.30 Hz from HVNR analysis and 3.25, 3.40 and 2.90 Hz from the HVIP analysis (see Tables 1 - 2). The directions of maxima varied within the range 135°-175° for HVNR and 125°-165° for HVIP. Conversely, strong differences appeared in peak amplitude obtained from HVNR and HVIP results and, while the estimate of maximum ellipticity derived from the HVIP analysis provided consistent results (between 6.1 and 6.5), strong variations were observed in the HVNR peak values (3.8, 9.8 and 6.7, for the three campaigns, respectively).

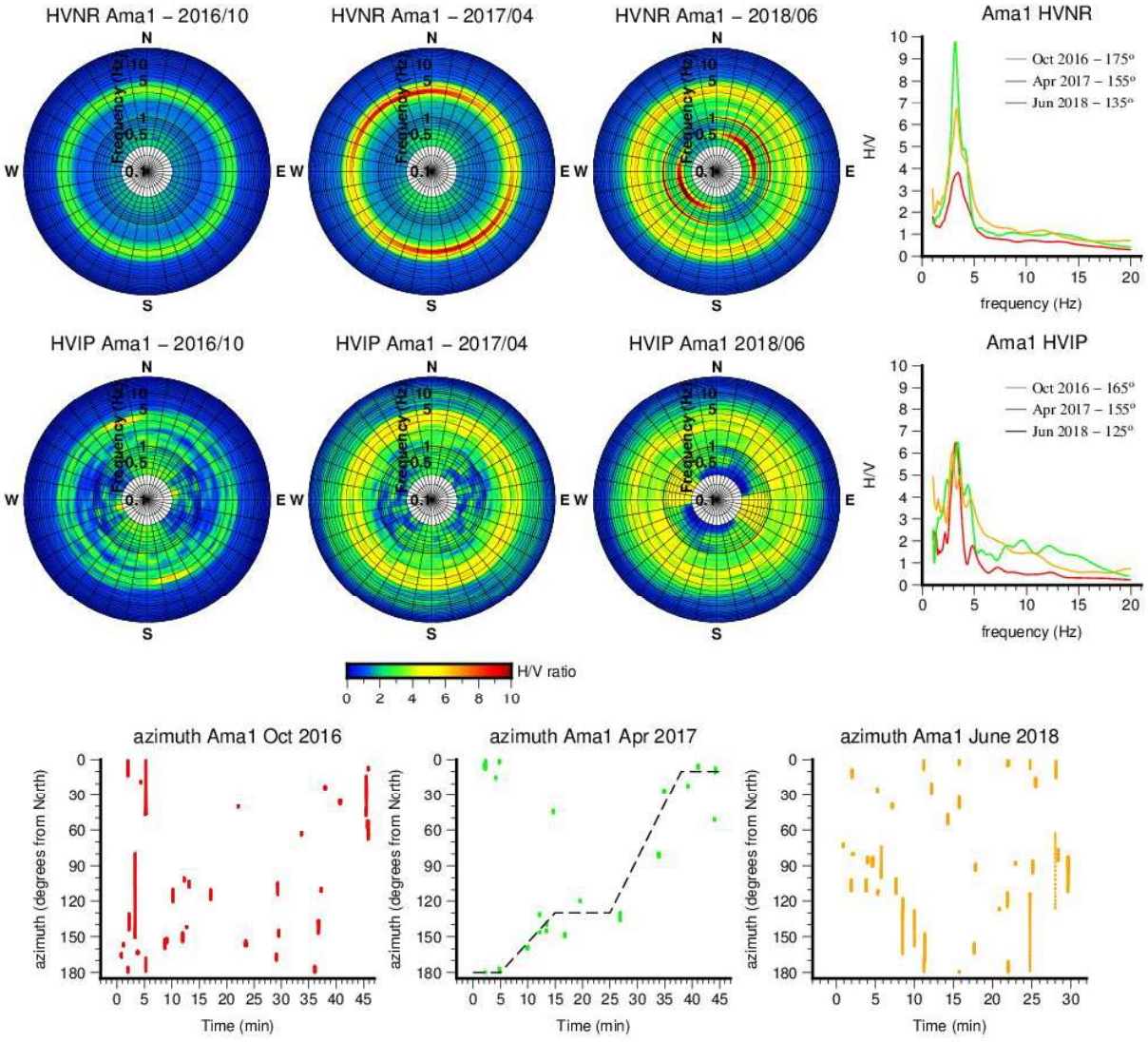

Fig. 7 – Polar diagrams of HVNR (top) and HVIP (centre) for the site Ama1, derived from the measurement campaigns of October 2016, April 2017 and June 2018. Diagrams to the right show, comparatively for all the campaigns, the H/V curves along the azimuths of major peaks. Diagrams at the bottom show the instantaneous estimates of Rayleigh waves azimuths (in degrees from North) at the peak frequencies (3.25, 3.40. and 2.90 Hz, for the three campaigns, respectively). For April 2017 measurements, the dashed line points out the observed step-wise rotation of Rayleigh wave polarization, attributed to a progressive migration of noise source related to the passage of a religious procession (see text for explanation).

The variability of HVNR results can be related to anomalous noise conditions during the 2017 and 2018 measurements. Indeed, the noise recording conditions in October 2016 were "quiet" because of the blockage of the main road exiting from the town to the north-west. By the time of the following measurement campaigns, the passage of people and/or vehicles was again possible. More specifically, the April 2017 measurements were carried out on Good Friday, whose celebration often involves a religious procession (named "Via Crucis") whose participants alternate walks and stops. During the noise measurements, a procession of this

type reached the area of Ama1 site through a road going from south to north. This is reflected in the results of the instantaneous polarization analysis, which show a stepwise rotation of the Rayleigh wave prevailing polarization, according to the stop and go pattern of the procession (see bottom-centre diagram in Fig. 7). Nothing of similar was observed in the previous or in the following measurement campaigns, for which Rayleigh wave polarization showed a random pattern at the peak frequencies (Fig. 7).

Overall, despite the anomalous condition of noise wavefield generation, the HVIP analysis provided perfectly consistent results (in terms of peak amplitude) with those of the other measurement campaigns. On the contrary, the estimates of the HVNR peak amplitudes were strongly altered, likely as an effect of a variable proportion of Rayleigh and Love waves, generated at short distances from the tromograph, which differently contribute to the horizontal and vertical component of the noise wavefield. Indeed, the results of the HVIP analysis revealed that, in comparison to the 2016 measurements, the percentage of samples classified as Love type was three times larger in April 2017 and twice as much in June 2018. This resulted in the increased HVNR peak values in the 2017 and 2018 recordings, whereas the HVIP maxima, obtained selecting only Rayleigh wave packets, remained unaffected. Additionally, these observations proved the effectiveness of the HVIP technique in recognizing the direction of Rayleigh wave propagation. This capability could be exploited in other applications of passive seismic surveys aimed at seismic velocity estimates (e.g., ReMi - Louie 2001), which are affected by uncertainties deriving from the lack of control on noise source azimuthal location.

Regarding the interior of the Red zone, the NW-most measurement station of the profile along the main street of the town, Ama12, was located about 100 m away from Ama1 (Fig. 1), in 13 m topographically higher area including conglomerates overlaid by siltstones. The measurements carried out in April 2017 and June 2018 consistently showed a major peak of Rayleigh wave ellipticity at a frequency between 3.7 and 4 Hz with amplitude between 4 and 5, i.e. lower than that at Ama1 (Fig. 8 - top). Resonance frequency is directly proportional to the shear-wave velocity Vs of the surface layer and inversely proportional to its thickness. Therefore, the slight increase of resonance frequency (from □3 to □4 Hz), despite the in situ observed thickening of the alluvial deposits from Ama1 to Ama12, implies a significant lateral increase of Vs of the surface material; this could be related to the presence of siltstone.

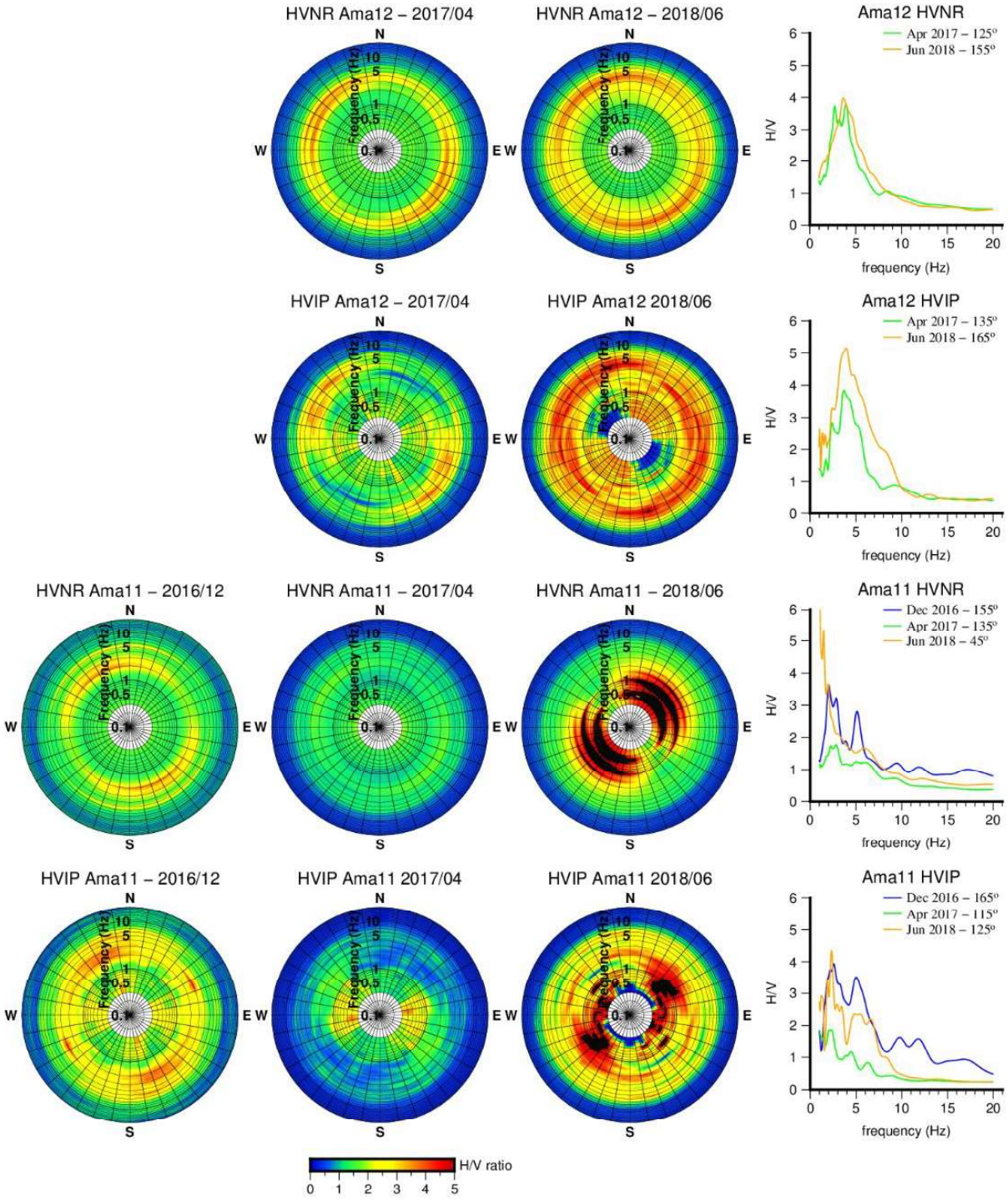

Fig. 8 – Polar diagrams of HVNR and HVIP for the sites Ama12 and Ama11, derived from three different measurement campaigns, as indicated in the diagram headers. Diagrams to the right show the H/V curves along the azimuths of major peaks for the three campaigns.

The next station Ama11 was located close to the clock tower, the only historical building in the Red zone survived to the earthquake (see the leftmost photo in Fig. 1). The results obtained from repeated measurements showed considerable variations. While the pattern of the polar diagram for the results derived from the

December 2016 recordings was consistent with those of the other stations of the Red zone, with a significant directional maximum at 2-2.5 Hz in NNW-SSE direction, the subsequent measurement campaigns produced rather anomalous outcomes (Fig. 8 – bottom). The analysis of the April 2017 noise data resulted in abnormally low (H/V < 2) values of spectral ratios and Rayleigh wave ellipticity, possibly due to a combination of weak energisation of noise wavefield with a not optimal coupling of tromograph with ground. The 2018 recordings were affected by an evident artificial NE- polarized signal, with strong peaks at 0.5, 1.0 and 1.5 Hz, which was subsequently recognized as an effect of instrument malfunction. However, despite the overlapping of this artificial signal, the HVIP analysis was still able to point out a significant peak, comparable with that resulting from the 2016 measurements.

Overall, the results of HVIP analysis indicated a lower resonance frequency at Ama11 than at Ama12 (2.3-2.6 Hz against 3.7-4.0 Hz) and, neglecting the 2017 data, a comparable amplitude (3.9-4.4 against 3.8-5.2). Considering that the altitude at Ama11 is about 10 m higher than at Ama12, the reduction of resonance frequency can be related to the increase in the thickness of the alluvial terrace deposits without lateral variations of velocity.

A similar pattern can be recognized at the remaining stations of the Red zone NW-SE profile (Ama10, Ama9, Ama8; Fig 1). The results shown in Figs. 9, 10 and 11, demonstrate a major peak of Rayleigh wave ellipticity in the band 2-4 Hz, whose frequency, however, first increases to 3.0-3.4 at Ama10, then returns to a value similar to Ama11 (2-2.6 Hz, for both Ama9 and Ama8). The higher frequency maximum at Ama10 could be linked to a reduced thickness of the terrace deposit or a lateral increase in S-wave velocity. As all the above stations are at elevation similar to or only slightly higher than Ama11, we can infer that either the local substratum depth (and so the thickness of the alluvial terrace) or the velocity of the terrace deposits velocity are different at Ama10.

In general, one can notice that peak amplitudes resulting from the HVIP analysis of noise recordings acquired at different times were quite consistent, whereas HVNR analysis occasionally provided considerably different values (e.g., at Ama9 and Ama8: see Figs. 10-11). Thus, conclusions concerning peak amplitudes should be drawn only from the HVIP results.

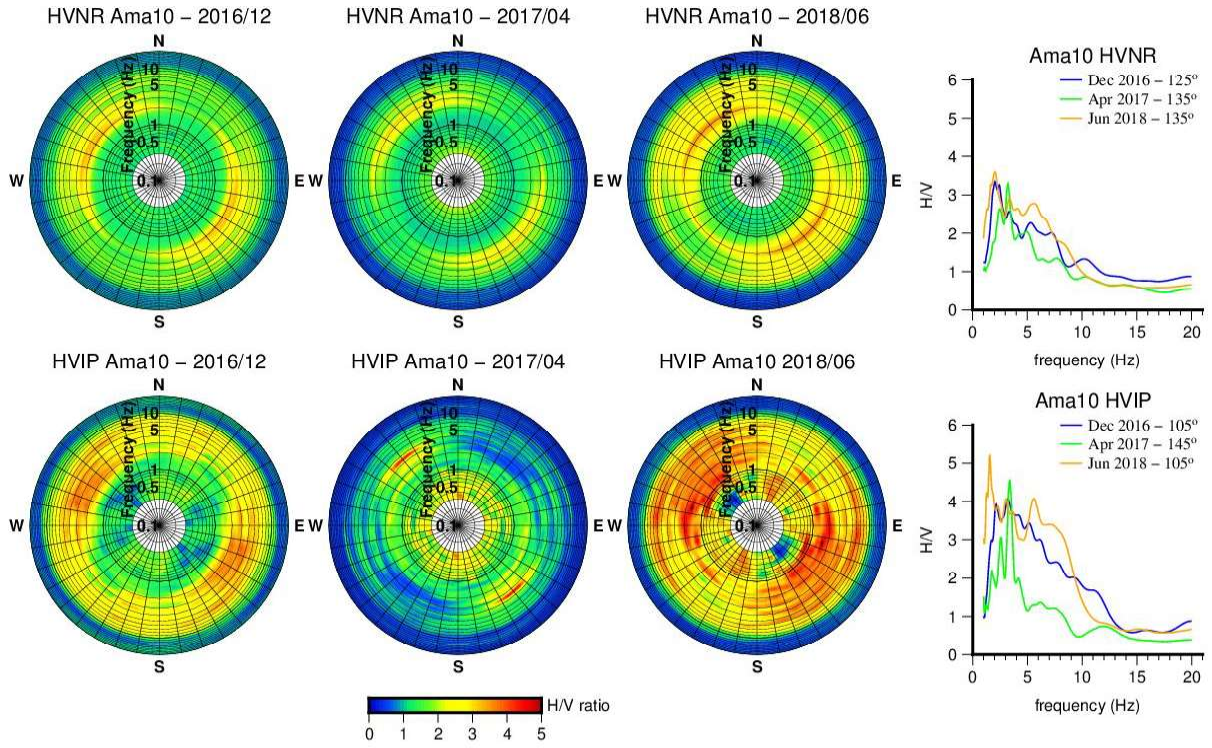

Fig. 9 – Polar diagrams of HVNR and HVIP for the site Ama10, derived from three measurement campaigns, as indicated in the diagram headers. Diagrams to the right compare the H/V curves along the azimuths of major peaks for the three campaigns.

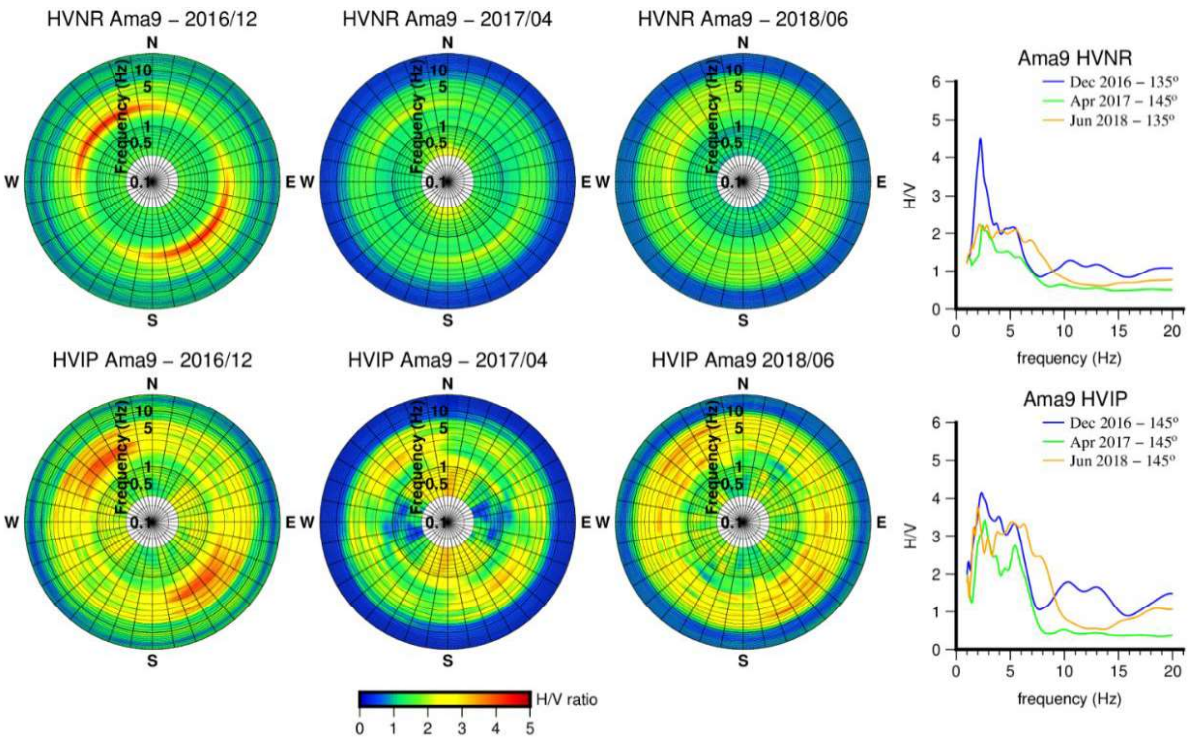

Fig. 10 – Polar diagrams of HVNR and HVIP for the site Ama9, derived from different measurement campaigns, as indicated in the diagram headers. Diagrams to the right compare the H/V curves along the azimuths of major peaks for the different campaigns.

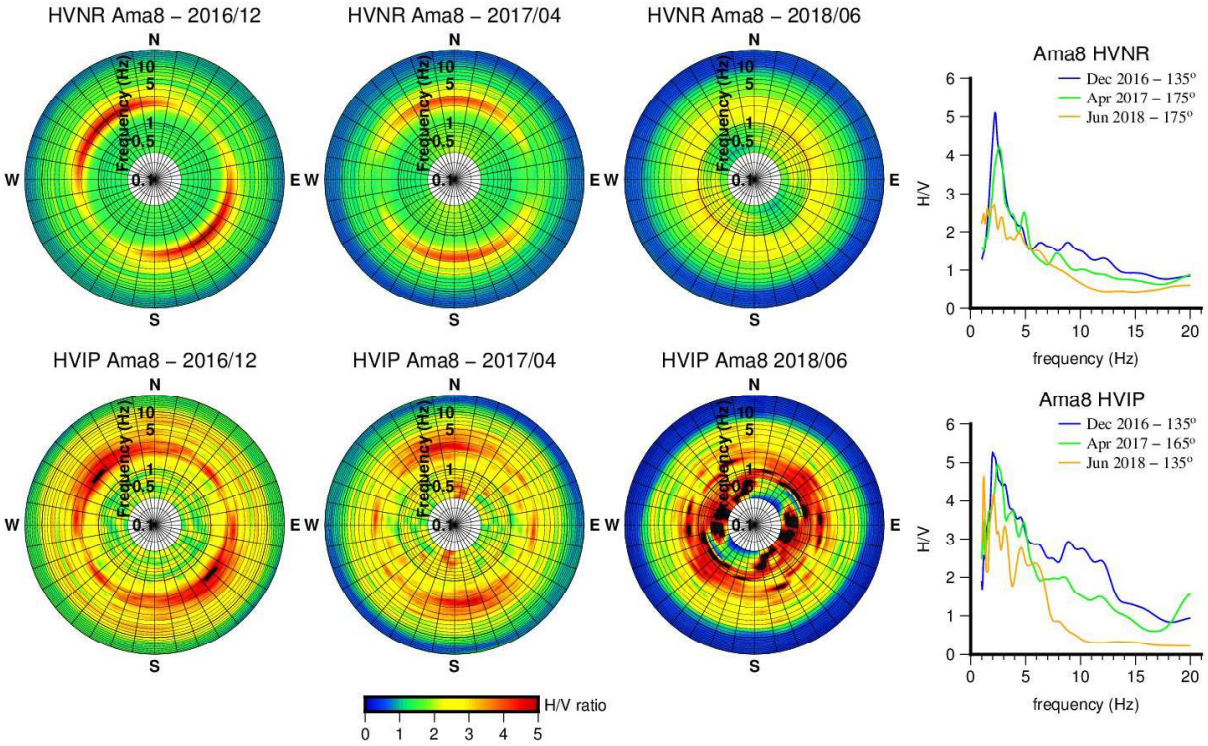

Fig. 11 – Polar diagrams of HVNR and HVIP for the site Ama8, derived from three different measurement campaigns, as indicated in the diagram headers. Diagrams to the right compare the H/V curves along the azimuths of major peaks for the three campaigns.

The peak amplitude of Rayleigh wave ellipticity at Ama8 was higher than at Ama9 (4.2 -5.3 against 3.4-4.2) for similar frequencies (2.0-2.45 Hz and 2.0-2.65 Hz, respectively). Since the similarity of resonance frequency implies that velocity and thickness of the surface layer are similar at these stations, the amplitude differences suggest a lateral variation in the substratum properties. We interpret the variation to be caused by an increase of the impedance contrast at Ama8 as an effect of a lateral passage to a stiffer lithology at the top portion of the flysch substratum.

5.3 The "Yellow" zone

Within the "Yellow zone", the H/V curves obtained at Ama5 showed a similar pattern to that of the reference Ama2, located about 150 m to the east (Fig. 1). In particular, we detected a major directional peak at 2-2.5 Hz and a secondary isotropic one at 9-10 Hz, but without the supplementary peak around 5 Hz (Fig. 12). The amplitudes of Rayleigh wave ellipticity were also quite consistent both for the major peaks (3.5-4.5 at Ama2, 4.3-4.4 at Ama5) and for the secondary ones (3.4-4.1 for Ama2 and 3.5-4.2 for Ama5). The lower resonance frequency, similar to that observed in the closest "Red zone" stations, could be attributed to the impedance

contrast between the terrace deposits and the flysch substratum. The higher frequency peak could be related to the effect of the local presence of a thin layer of surficial material at the top of the terrace deposits.

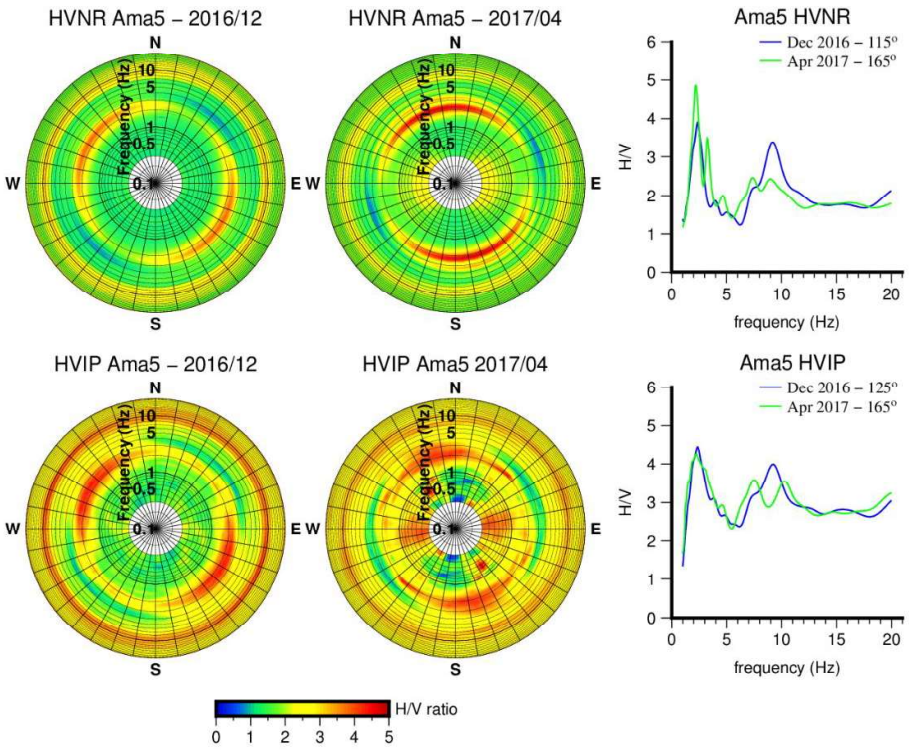

Fig. 12 – Polar diagrams of HVNR and HVIP for the site Ama5, derived from two different measurement campaigns, as indicated in the diagram headers. Diagrams to the right show comparatively the H/V curves along the azimuths of major peaks for the two campaigns.

In the southern part of the Yellow zone, the measurements were carried out at stations Ama6 and Ama7 (Fig. 1) during the last three campaigns. The 2018 measurements at Ama7 appear contaminated by the same effect of the instrument malfunction observed at Ama11 (Fig. 13). However, also in this case the HVIP analysis proved capable to recover Rayleigh wave properties consistent with those observed during the previous campaigns.

The recordings from these two stations showed a major peak of Rayleigh wave ellipticity with characteristics similar to those observed at Ama5, i.e., approximately NW-SE oriented, at frequency between about 2 (at Ama7) and 3 Hz (at Ama6), and with comparable amplitude (between 4.3 and 4.6). The secondary peak around 9-10 Hz was absent (at Ama6) or weaker (at Ama7) and we infer that the thin layer responsible for this effect could be discontinuous in the area between the reference station and the Yellow zone.

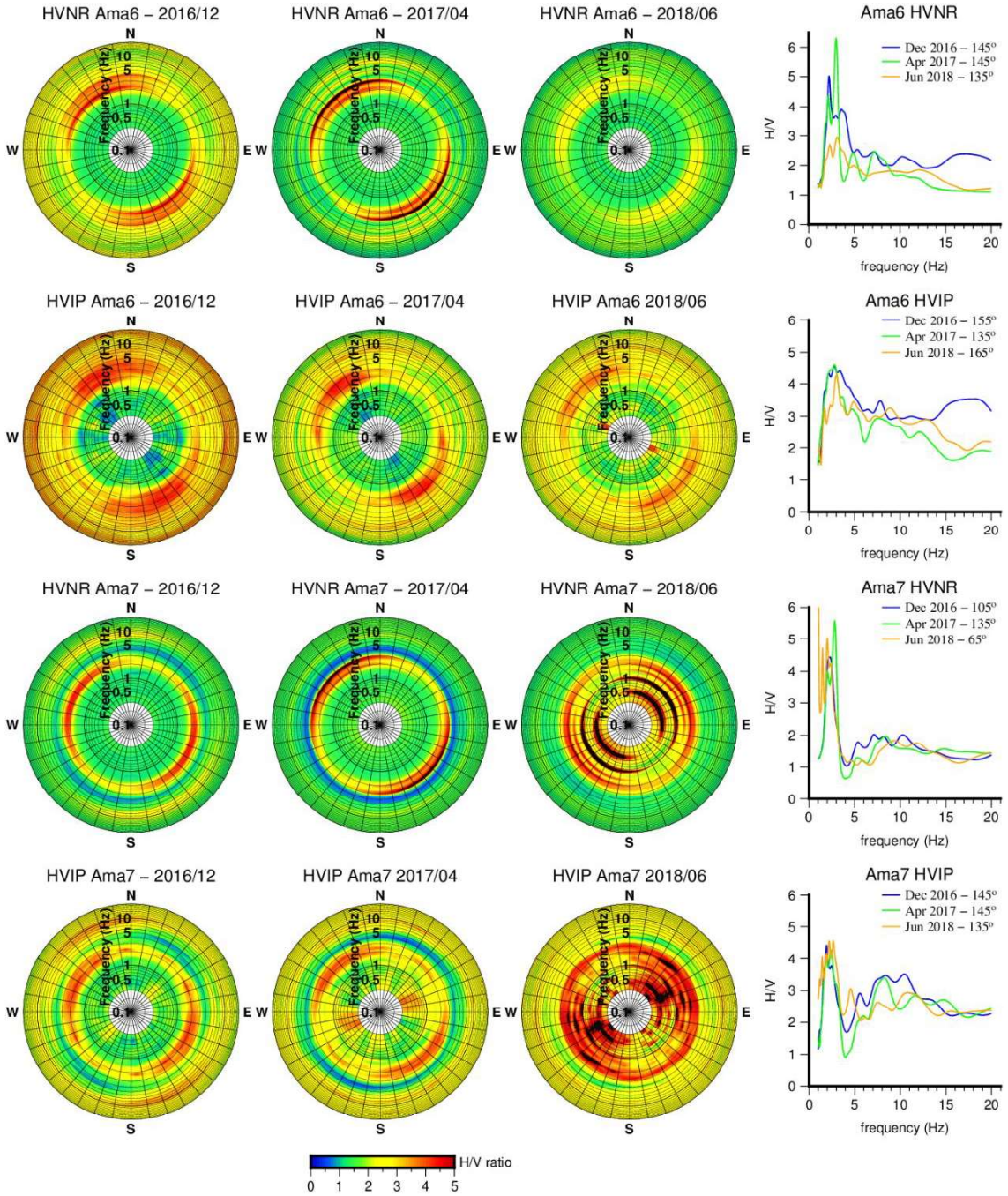

Fig. 13 – Polar diagrams of HVNR and HVIP for the sites Ama6 and Ama7, derived from three measurement campaigns, as indicated in the diagram headers. Diagrams to the right compare the H/V curves along the azimuths of major peaks for the three campaigns.

5.4 The eastern zone

Apart from the reference Ama2, two additional measurement stations were set up in the less damaged area to the east of the Red and Yellow zones, The station Ama3 was located in the middle of the area, inside the garden of a villa, whereas Ama4 was in the eastern outskirt of the town (Fig. 1). The noise recordings were obtained

during the first (October 2016) and the last (June 2018) measurement campaigns.

At Ama3, the HVNR results did not reveal any peak significantly exceeding an amplitude of 2. The HVIP analysis showed a major peak at 8-9 Hz in the 2016 noise recordings, whose persistence, however, was not confirmed by the 2018 measurements (Fig. 14). Thus, the peak at around 2.2 Hz with amplitude of 3.2-3.5 was the only one that showed similar characteristics in both measurement campaigns, (although with different directions, which suggests the absence of a site-specific response directivity).

A peak with slightly higher frequency and amplitude (2.8 Hz and 3.6, respectively, on average) was identified at Ama4, both from the results of HVNR and HVIP analysis. The characteristics of these peaks are quite consistent with that of the lower component of the 2-5 Hz resonance band at Ama2 in the westernmost zone of the less damaged area (Fig. 1). In particular, the amplitudes of the observed peaks are very similar if one compares the outcome of the coeval measurements.

6. Discussion

6.1 Spatial variation of site resonance properties

Figure 15 shows a summary of the results of ambient noise analysis obtained through the HVIP technique. We consider the outcomes of this kind of analysis as capable to provide more comprehensive information on site response properties with respect to the information derived from resonance frequencies only. Indeed, it had been observed that Rayleigh wave ellipticity peak amplitudes are correlated to amplification factors (cf. Konno and Ohmachi, 1998 and Figs. 15, 17 therein; Kawase et al., 2019), as effect of ellipticity increase with the increase of impedance contrast between overburden and bedrock.

In this study, the HVIP method applied to measurements repeated at different times provided more consistent values of H/V peak amplitudes, in comparison to the HVNR approach. This is likely due to the fact that spectral ratios averaged over time windows of 20-30 seconds are strongly influenced by variation of composition of the noise wavefield, which can include other wave types in addition to Rayleigh waves.

In general, we observed that the HVIP peak amplitudes are frequently larger than the HVNR ones. Similar results were obtained in previous comparative tests (Del Gaudio, 2017, Del Gaudio et al., 2018). This can be explained as effect of a considerable contribution of body waves to the vertical component of noise.

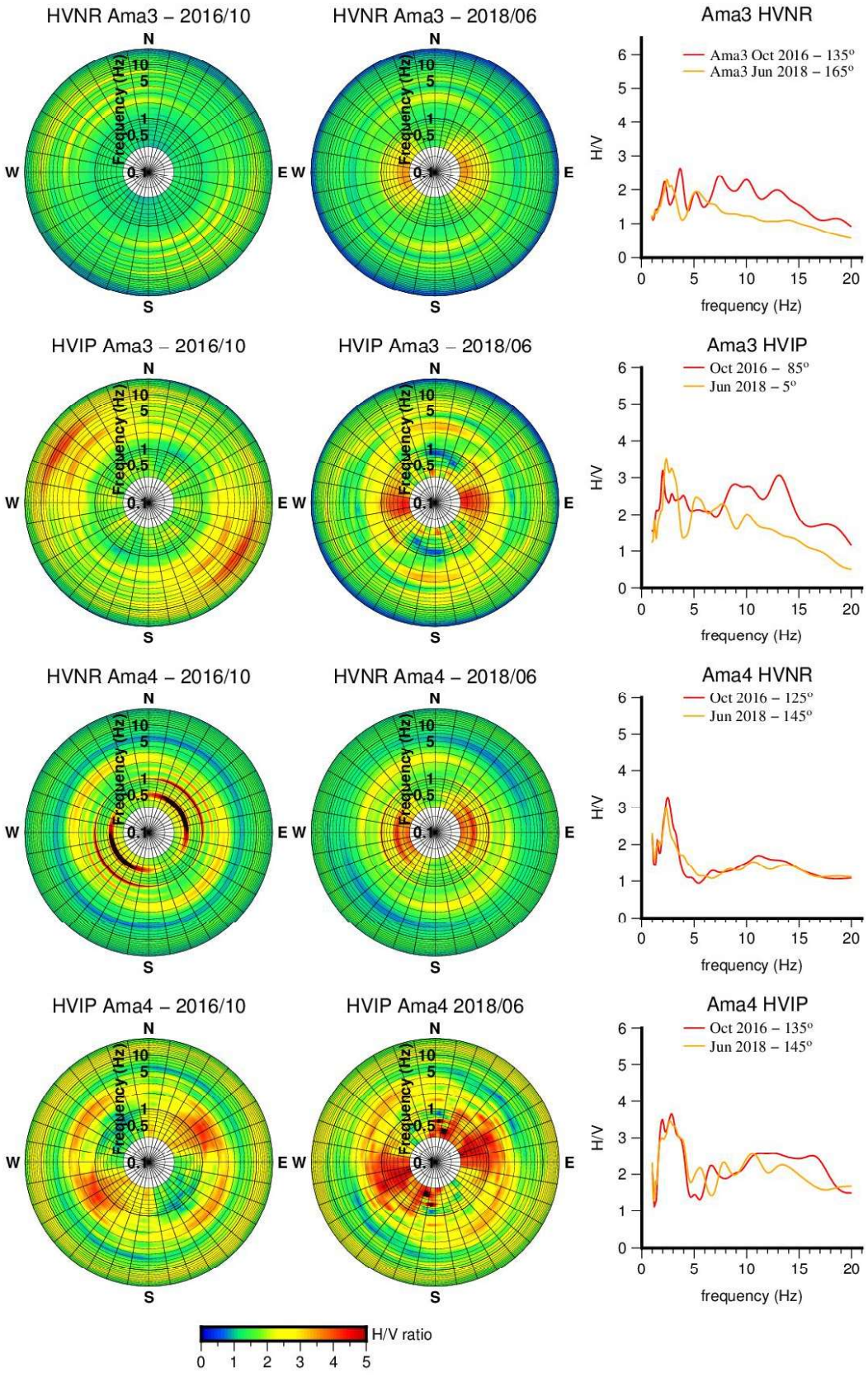

Fig. 14 – Polar diagrams of HVNR and HVIP for the sites Ama3 and Ama4, derived from two measurement campaigns, as indicated in the diagram headers. Diagrams to the right compare the H/V curves along the azimuths of major peaks.

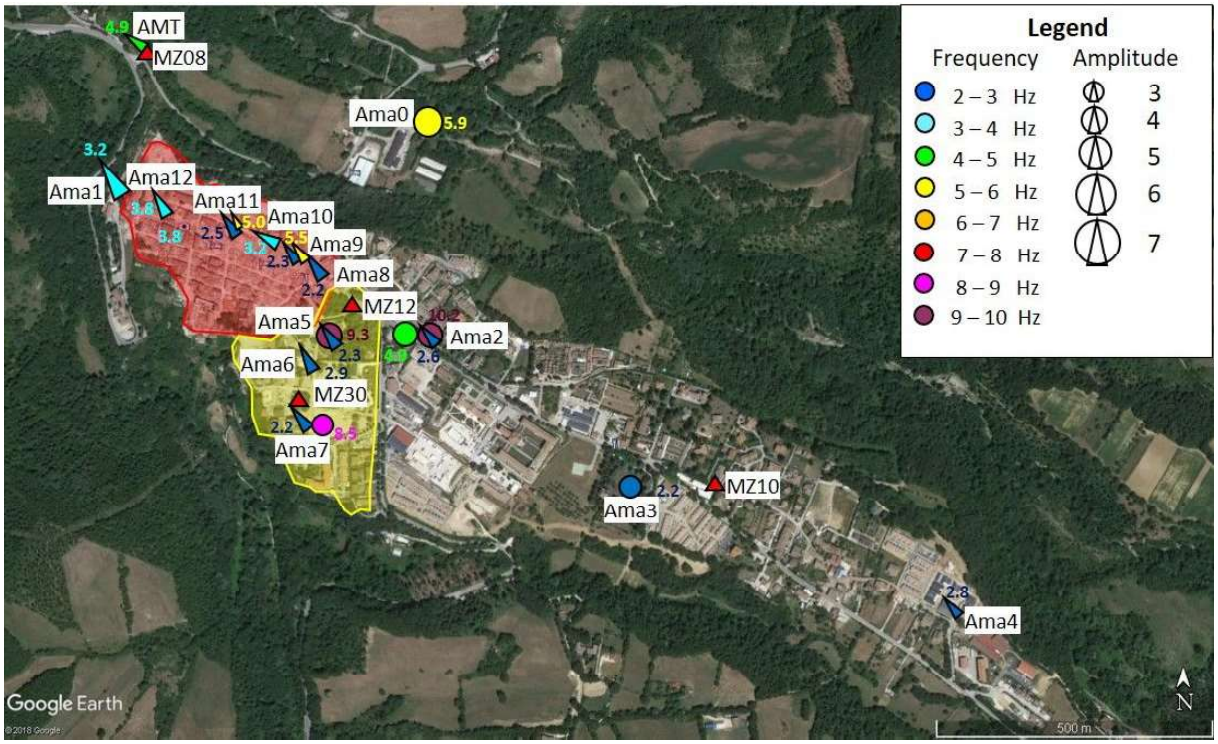

Fig. 15 – Summary of results of the HVIP analysis of ambient noise recordings codified in terms of peak frequencies, amplitudes and directions, according to the top-right legend. Diversified symbols, whose colours represent the frequencies (also printed next to the symbol) of maximum Rayleigh wave ellipticity, mark directional properties at each measurement station. Arrowheads indicate the direction of maximum at sites characterised by a clear persistent directivity, circles denote sites with low (< 1.5) R index or with variable maximum directions. Symbol size scaled according to the amplitude of the H/V maximum. Red triangles mark the locations of accelerometer stations whose earthquake recordings were used in the study of Milana et al. (2019).

Our instantaneous polarization analysis showed that, within a noise recording, only a minor portion presents a clear Rayleigh- or Love-type polarization (generally 1-2% for Rayleigh waves and little more for Love waves). Most of a recording shows randomly oriented directions of elliptical trajectory axes (cf. Del Gaudio 2017 and Fig. 1 therein), likely as effect of the overlapping of waves of different type. Only when more energetic packets of Rayleigh or Love waves prevail on the background noise, one can recognize the corresponding type of polarization. In particular, around the site resonance frequencies, for which the vertical components of Love and Rayleigh waves are null or minimum, body waves are likely to give a major contribution to the vertical component, as also observed in some studies aimed at investigating the noise composition (cf. Bonnefoy-Claudet et al. 2006 for a review). Therefore, in the calculation of spectral ratios over time windows of 20-30 s, the presence of a considerable amount of body waves contributing to the vertical component of ground vibration, tends to reduce the H/V peak amplitude.

Therefore, we prefer to use peak amplitudes of HVIP curves, which isolate just the noise recording portions with a clear Rayleigh-type polarization, as a more reliable indicator of lateral variation of site response properties through the study area.

Overall, considering the profile crossing the Red zone, peak values of Rayleigh wave ellipticity revealed resonance frequencies between 2 and 4 Hz, with slightly higher frequency towards the north-western end of the zone. This is possibly related to the lateral thinning of the Amatrice terrace deposits. Higher frequencies encountered at the centre of the Red zone could be linked to lateral variations in the terrace deposit characteristics (mechanical properties or thickness). Occasionally, a secondary maximum was observed at 5-6 Hz (e.g., at stations Ama11 and Ama9), which could be related to the locally present thin layer of surficial material. All these peaks had an apparent directional character, with an approximately NW orientation, and amplitudes higher at the NW and SE ends of the "Red zone" than in its inner part. This can be related to the lateral variations in stiffness of the substratum (flysch lithology), which result in changes in impedance contrast with the surface deposits.

The stations in the "Yellow zone" showed similar characteristics, with a major peak at 2-3 Hz having amplitude comparable with the average amplitude of the "Red zone" peaks. Additional higher frequency peaks (8-10 Hz) with a more isotropic character (mean R index <1.5: see Table 2) were locally recognized (at Ama5 and Ama7, but not at Ama6); this could be related to the presence of laterally discontinuous softer surface layers. Overall, no clear difference in site response emerged between the Red and Yellow zones, which suffered a different level of damage. Indeed, if one consider the average values of ellipticity peaks derived from different measurements at the same station, peak frequencies in the Red zones were comprised between 2.2 and 3.8 Hz, against a range of 2.2 - 2.9 Hz in the Yellow zone, whereas peak amplitudes were from 3.8 to 6.4 in the Red zone and from 4.4 and 4.5 in the Yellow one. Thus, in some cases, resonance properties were found more variable within the Red zone (e.g. Ama1 and Ama9) than between a couple of sites belonging to the Red and Yellow zone (e.g. Ama11 and Ama5: see Table 2).

With regard to the central and eastern part of the town, our data are too limited to draw general conclusions. However, one can notice that, at the reference station Ama2, the ellipticity peak amplitudes derived from measurements in wet seasons (when the amplitudes are higher) were comparable to the mean values obtained

in the same seasons for the Red and Yellow zones. This suggests that, at least at this site, amplification may not be significantly lower than in the most damaged zone.

6.2 Comparison with previous studies

Milana et al. (2019) carried out a comparison between the results of analysis of ambient noise, conducted with the Nakamura's method, and the results of the analysis of standard spectral ratios (SSR) of the accelerometer recordings acquired at a number of stations (mostly temporary) located in the Amatrice area. The SSR analysis consists of the calculation of mean spectral ratios between recordings of the same earthquakes acquired at study sites suspected to be affected by amplification phenomena, and at a nearby reference site (cf., Borcherdt 1970).

One of the Milana et al. (2019) accelerometer stations, named MZ08, coincides with AMT (Figs. 1-15) and, at this site, our HVIP results appear quite consistent with the outcomes of the SSR analyses. The SSR values in the cited publication show a significant spectral amplification (by a factor larger than 2) between 3 and 6 Hz. This is also the frequency band for which the HVIP analysis provides the maximum ellipticity values (H/V > 3: see Fig. 5). Few other accelerometer sites considered by Milana et al. (2019) resulted to be relatively close to some of our noise measurement stations. In particular, two accelerometer stations (named MZ12 and MZ30), were located in the "Yellow zone" 70 and 50 meters away from Ama5 and Ama7, respectively, and one (MZ10) 150 metres away from Ama3 (see Fig. 15 for their location). Overall, there is a good agreement between the lower frequency peaks of Rayleigh wave ellipticity (around 2 Hz) shown by the HVIP analysis and major resonance frequencies revealed by the SSR analysis. A good correlation also exists between the HVIP peak amplitudes and amplification factors: both were lower at Ama3 (on average, around 3.4 and 2, respectively) and higher at Ama5 and Ama7 (4.4 and around 4, respectively). Additional higher frequencies resonances are also shown by both the kind of analyses, although at frequencies differing by 1-2 Hz in the two kind of analyses. Such discrepancies, however, considering the not perfect coincidence of the measurement point locations, could reflect very local variations in surface material properties and/or in their thickness.

Regarding the comparison with the results obtained by Milana et al. (2019) from standard ambient noise analysis, there is a substantial consistency in recognizing site resonance within the Red-Yellow zones as occurring prevailingly at frequencies between 2 and 3 Hz. However, the observed peak amplitudes are

occasionally quite different and the directions of maximum diverge significantly from those found in our study. For instance, at station MZ12, for the 2 Hz resonance frequency revealed by the SSR analysis by Milana et al. (2019), their results of the HVNR analysis indicate a weak peak with amplitude only slightly larger than 2, against values of 3.9-4.8 derived from our measurements. These differences may not be related to seasonal changes, because the measurement repetitions conducted within few days (under different weather conditions) revealed large amplitude variations (Milana et al. 2019). All this confirms the instability of HVNR peak amplitudes pinpointed by our multitemporal analysis. Indeed, the amplitudes can differ considerably between measurements carried out at different time, as an effect of changes in the noise wavefield composition.

There are also inconsistencies regarding the maxima directions, which in all our measurement campaigns resulted prevailingly NW-SE oriented, whereas Milana et al. (2019) reported orientations close to NE-SW direction. The observed variations could reflect wavefield polarization properties controlled by noise sources, changing under different environmental conditions (e.g. between measurements affected by anthropic activity during the day, as in our work, and noise of natural origin at night, as in some measurements acquired by Milana et al. 2019). This would imply the lack of a pronounced anisotropy in site response that could generate a clear site-specific directivity of maximum ground shaking.

6.3 Influence of soil-structure interactions

The uncertainties affecting the interpretation of the results of the analysis of ambient noise recorded in an urbanized area can in part arise from the possible influence of dynamic soil-structure interactions on noise wavefield (e.g., Wirgin and Bard, 1996; Gallipoli et al., 2004). We had the opportunity to verify this issue in three cases, i.e., at the stations Ama12, Ama6 and Ama2, where ambient noise recordings were obtained before and after the demolition of nearby buildings

At Ama12, the first ambient noise records were acquired on April 2017, at a site few meters away from two-story buildings, which were demolished before the following measurement campaign of June 2018. At Ama12, the main resonance frequency obtained from noise analysis was around 4 Hz, i.e., higher than at the two closest stations (3 Hz at Ama1 and 2-2.5 Hz at Ama11; see Figs. 7-8) set up along the profile through the Red zone (Fig. 1). Although 4 Hz frequency, in principle, could correspond to the building resonance, the fact that the peak frequency observed before and after the building demolition was the same (Fig. 8), supports the

interpretation of the observed spatial variation of resonance frequency as due to lateral variation in the terrace deposit properties (velocity or thickness).

A second case is that of the Ama6 site, located in the "Yellow zone" about 10 m from the three-story building of the local "Carabinieri" (military police) headquarters (bottom photo in Fig. 1), which was demolished between the December 2016 and April 2017 measurement campaigns. Significantly, the HVIP provided practically the same peak amplitudes at the same resonance frequency in all the measurement campaigns (Fig. 13), regardless the presence/absence of the Carabinieri building. Thus, also in this case, the resonance peak observed can be attributed to the soil response.

Finally, regarding the Ama2 reference site, by the time of the last measurement campaign (June 2018), the nearby three-story hotel building (top-centre photo in Fig. 1) had been demolished. Nevertheless, the HVIP curve based on June 2018 recordings was very similar to that obtained from the first campaign (October 2016) and differed from those of April 2017 and December 2016, only for the displacement of the peak, within the resonance band of 2-5 Hz, towards its upper bound (see Fig, 4). Thus, again, the resonance properties variations (frequency and amplitude) observed among different measurements are more likely related to a seasonal variation in the site response (see the following section) rather than to the effect of soil-structure interaction.

Overall, we did not find any clear evidence that would indicate that the observed resonance properties are related to perturbations induced into the soil by building vibration. Gallipoli et al. (2004) reported that, for ordinary building, the influence of soil-structure interaction generally is negligible at a distance equal to the building height, even though can be much more areally extended in presence of high structures with deep foundations. In the cases of Ama6 and Ama2, the distance between the measurement points and the buildings was comparable to the buildings' height, so that the contribution of their vibration to the ambient noise may have been negligible. At Ama12, however, the distance is smaller than the buildings height. In this case, the absence of a soil-structure effect could be due to the serious damage suffered by the buildings and their foundations, which reduced their rigidity and coupling with soil, thereby the efficiency of the transmission of building vibrations to the soil. Indeed, physical and numerical tests by Tuladhar et al. (2008) indicated that lateral cyclic loading can cause a degradation of mechanical properties of both soil and foundation structures, and even the opening of gaps between soil and foundation, which reduce the foundation capacity of transferring stress to the soil.

6.4 Evidence of seasonal variations

The changes in the ellipticity curve observed at the reference site Ama2 between the different measurement campaigns seem to follow a seasonal/climatic cycle, i.e., going from wetter (winter – spring) to drier (summer –early autumn) seasons. To verify a possible connection with the periodical variation of water content in the alluvial terrace deposits, we inverted the ellipticity curve in terms of subsoil velocity, by using the package "Dinver" (Wathelet, 2005) produced by the project "Geopsy" (www.geopsy.org).

The inversion of ellipticity curves is not univocal and independent constraints are needed to limit the number of solutions. In our case, one constraint is given by the thickness of the terrace deposit, which was inferred to be within a range of 30-35 m from the field geological observations and borehole stratigraphies (see Fig. 2). Figure 16 shows the inversion results of two curves, averaged over those obtained from noise data acquired in wet seasons (December 2016 and April 2017) and in drier ones (October 2016 and June 2018).

The misfit between the theoretical and experimental values of Rayleigh wave ellipticity is measured through the root mean square of their differences, normalized by the standard deviation of the measurement results. It was possible to obtain an excellent fitting for the two curves, maintaining the same vertical distribution of S-wave velocity (Vs) and slightly modifying the P-wave (Vp) profile. Although the Vp values within the terrace deposits are less well constrained by the data (especially for the "wet season" curve), we infer that the change in Rayleigh wave ellipticity curves can be simply explained in terms of variation of P-wave velocities at a depth range between 10 m and 30-35 m. In particular, the increase of ellipticity around 2.5 Hz between dry and wet seasons can be reproduced through an increase of the Poisson coefficient from 0.36-0.38 to 0.43-0.44, which, in turn, is consistent with an effect of water saturation of the alluvial terrace deposits.

Overall, these results indicate that seasonal/climatic variations can add some scattering around the correlation between amplification factors and ellipticity peak amplitudes. This influence should be taken into account when inferring relative variations of amplification from ellipticity and suggests the need to base such inferences on noise recordings obtained in the same season.

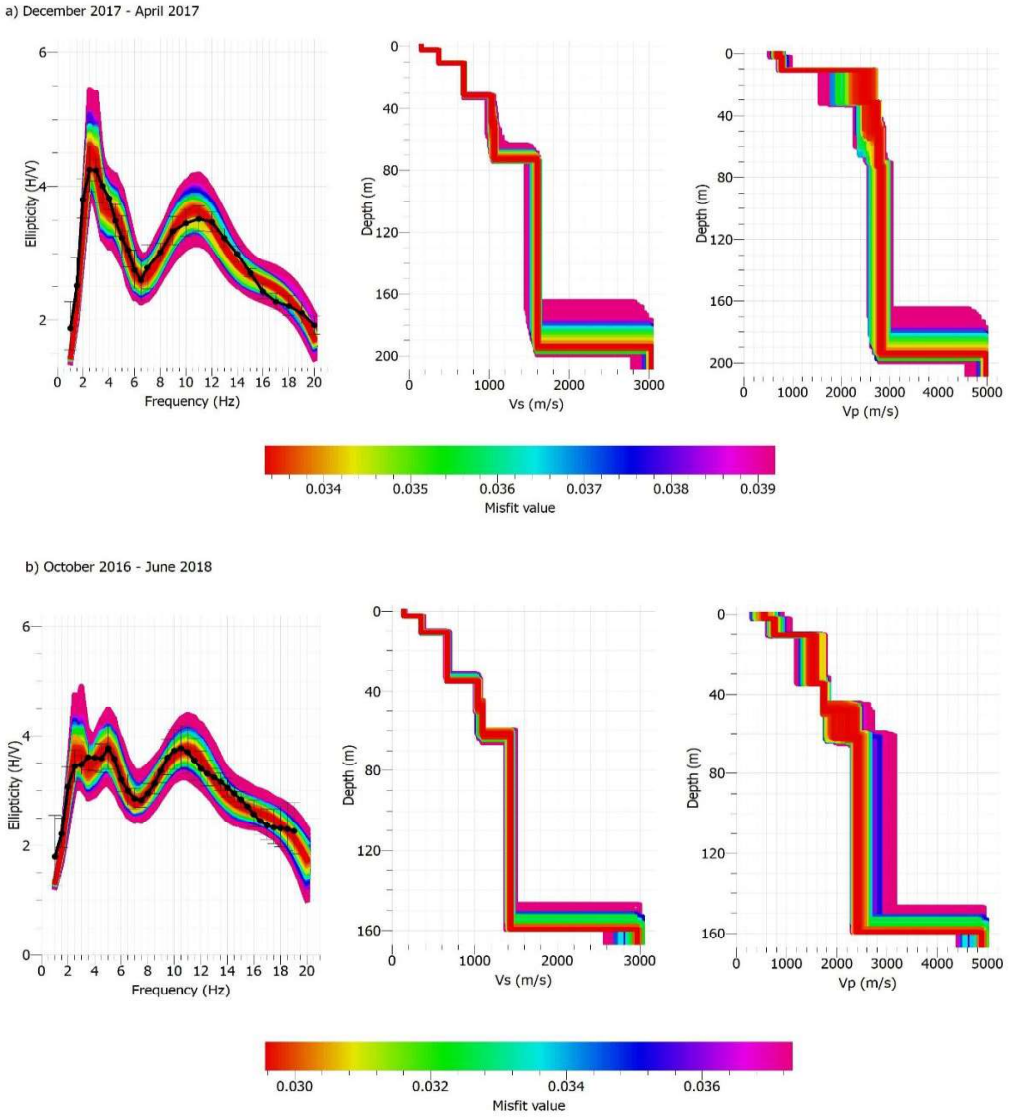

Fig. 16 – Results of the inversion of mean ellipticity curves at station Ama2, calculated by averaging the curves obtained in: a) wetter season (December 2016 and April 2017); b) drier periods (October 2016 and June 2018). In the left diagrams, black dots represent the experimental values (with error bars corresponding to uncertainties within one standard deviation), whereas the differently coloured curves represent theoretical models characterized by different misfit according to the chromatic scale. Vertical velocity profiles are shown with the corresponding misfit colour, in the middle and right diagrams, for S-wave and P-wave, respectively.

7. Conclusions

The investigation of the site response characteristics at 14 sites of the Amatrice urban area, within the zones severely damaged by the 2016 earthquake, revealed significant resonance phenomena at frequencies of 2 – 5 Hz. Such frequencies are relevant for the dynamic response of the locally common construction typology

(buildings of 2 – 5 floors). However, the differences in site response properties (in terms of frequency and amplitudes) do not appear correlated with the severity of the observed damage. Therefore, other factors need to be considered to explain the spatial variability of the earthquake effects.

Comparing our results with those of a recent previous study (Milana et al., 2019), a good agreement was found in terms of resonance frequency identification. However, considerable discrepancies emerged with regard to site response directivity. It is possible that these discrepancies reflect the presence of different environmental conditions during noise acquisition campaigns, with variable sources of polarized noise (anthropic or natural). This in turn may also indicate that, in reality, the site response at Amatrice does not have a clear directional character.

The adoption of a multi-temporal analysis of ambient noise recordings showed that, while the site resonance frequency identified through the standard Nakamura technique appeared quite stable, significant variations were observed in peak amplitudes of spectral ratios. The variations can depend on two factors: 1) the changes in noise wavefield composition under variable environmental conditions, with a different proportion of Rayleigh, Love and body waves; 2) seasonal variation of subsoil velocity, especially of the P-waves, in relation to the variation of water content in the Amatrice alluvial terrace deposits. This variability calls for caution in the use of the curves of horizontal-to-vertical spectral ratios in numerical inversion aimed at obtaining sub-soil velocity models. Particular attention should be paid to the definition of the velocity contrast between surficial deposits and substratum, which is mainly constrained by the curve peak amplitude.

The difficulties related to the changes in noise wavefield composition can be overcome through the employment of advanced data processing techniques, like the recently presented HVIP analysis, that are able to isolate, within the noise recordings, the contribution of the Rayleigh waves. At this regard, the HVIP technique proved capable to provide more stable estimates of the peak values of Rayleigh wave ellipticity and also to recognize the propagation direction of the recorded signals. The latter offers the opportunity of providing support to other passive seismic techniques, for which the lack of control on the signal propagation direction causes interpretative uncertainties. Moreover, the capacity of the new method to reveal relatively subtle variations of Rayleigh wave velocity related to seasonal/climatic change (for instance subsoil water content), opens new perspectives for its employment for monitoring purposes.

Acknowledgement

We are grateful to the Municipal Administration of Amatrice for allowing us to access to the "Red zone" during the measurement campaigns. A special thank you to Elio Ursini, of the L'Aquila Civil Protection Unit, for the assistance provided in organizing the field activity and in obtaining the authorization for the access to the restricted areas of Amatrice. The comments of the editor and two reviewers stimulated significant improvements of the paper.

References

Bard, P.Y., 1999: Microtremor measurements: a tool for site effect estimation?, in *The effects of surface geology on seismic motion*, pp. 1251–1279, ed. Irikura, K., Kudo, K., Okada, H. & Sasatani, T., Balkema, Rotterdam.

Bard, P.Y. & the SESAME Team, 2004: *Guidelines for the implementation of the H/V spectral ratio technique on ambient vibrations*. SESAME European research project WP12 – Deliverable D23.12, 62 pp, ftp://ftp.geo.uib.no/pub/seismo/SOFTWARE/SESAME/USER-GUIDELINES/SESAME-HV-User-Guidelines.pdf.

Bonnefoy-Claudet, S., Cotton, F. & Bard, P.-Y., 2006: *The nature of seismic noise wavefield and its implications for site effects studies – A literature review*, Earth-Sci. Rev., **79**, 205–227, doi: 10.1016/j.earscirev.2006.07.004.

Borcherdt, R.D., 1970: Effects of local geology on ground motion near San Francisco Bay, *Bull. Seism. Soc. Am.*, **60** (1), 29-61.

Castellaro, S. & Mulargia, F., 2009: *VS_{30} Estimates Using Constrained H/V Measurements*, Bull. Seism. Soc. Am., **99** (2A), 761–773.

Del Gaudio, V., 2017: *Instantaneous polarization analysis of ambient noise recordings in site response investigations*. Geophys. J. Int., **210**, 443–464, doi: 10.1093/gji/ggx175.

Del Gaudio, V., Coccia, S., Wasowski, J., Gallipoli, M.R. & Mucciarelli, M. 2008: *Detection of directivity in seismic site response from microtremor spectral analysis*, Nat. Hazards Earth Sys. Sci., **8**, 751-762, doi: 10.5194/nhess-8-751-2008

Del Gaudio, V., Muscillo, S. & Wasowski, J., 2014: *What we can learn about slope response to*

earthquakes from ambient noise analysis: an overview. Eng. Geol., **182**, 182–200, doi:10.1016/j.enggeo.2014.05.010.

Del Gaudio, V., Luo, Y., Wang ,Y. & Wasowski, J., 2018: *Using ambient noise to characterise seismic slope response: The case of Qiaozhuang peri-urban hillslopes (Sichuan, China)*. Eng. Geol., **246**, 374-390, doi: 10.1016/j.enggeo.2018.10.008.

Gallipoli, M. R., Mucciarelli, M., Castro, R.R., Monachesi, G. & Contri, P., 2004: *Structure, soil–structure response and effects of damage based on observations of horizontal-to-vertical spectral ratios of microtremors*. Soil Dyn. Earthq. Eng., **24**, 487–495, doi:10.1016/j.soildyn.2003.11.009.

Kawase, H., Nagashima, F., Nakano, K., Mori, Y., 2019: *Direct evaluation of S-wave amplification factors from microtremor H/V ratios: Double empirical corrections to "Nakamura" method*. Soil Dyn. Earthq. Eng., 126, 105067, doi: 10.1016/j.soildyn.2018.01.049.

Konno, K. & Ohmachi, T., 1998: *Ground motion characteristics estimated from spectral ratio between horizontal and vertical components of microtremor*. Bull. Seism. Soc. Am., **88** (1), 228-241.

Louie, J.N., 2001: *Faster, Better: Shear-Wave Velocity to 100 Meters Depth from Refraction Microtremor Arrays*. Bull. Seism. Soc. Am., **91**, 347-364.

Milana, G., Cultrera, G., Bordoni, P., Bucci, A., Cara, F., Cogliano R., Di Giulio, G., Di Naccio, D., Famiani, D., Fodarella, A., Mercuri, A., Pischiutta, M., Pucillo, S., Riccio , G. &, Vassallo, M., 2019: *Local site effects estimation at Amatrice (Central Italy) through seismological methods*. Bull. Earthq. Eng., doi: 10.1007/s10518-019-00587-3.

Morozov, I. B. & Smithson, S. B. 1996. Instantaneous polarization attributes and directional filtering, *Geophysics*, **61**, 872-881.

Nakamura, Y., 1989: *A method for dynamic characteristics estimation of subsurface using microtremor on the ground surface*. Q. Report Railway Tech. Res. Inst., **30**, 25–33.

Perron, V., Gélis, C., Froment, B., Hollender F., Bard, P.-Y., Cultrera, G. & Cushing E. M., 2018: *Can broad-band earthquake site responses be predicted by the ambient noise spectral ratio? Insight from observations at two sedimentary basins*. Geophys. J. Int., **215**, 1442–1454, doi: 10.1093/gji/ggy355.

Tuladhar, R., Maki, T. & Mutsuyoshi, H., 2008: *Cyclic behavior of laterally loaded concrete piles embedded into cohesive soil*. Earthquake Eng. Struc., **37**, 43-59, doi: 10.1002/eqe.744.

Wathelet, M., 2005: *Array recordings of ambient vibrations: surface-wave inversion*. PhD thesis, Université de Liège, Belgium

Wirgin, A. & Bard, P.-Y., 1996: *Effects of Buildings on the Duration and Amplitude of Ground Motion in Mexico City*. Bull. Seism. Soc. Am., **86** (3), 914-920.